European Journal of Wood and Wood Products (2026) 84:58
https://doi.org/10.1007/s00107-026-02412-6

ORIGINAL ARTICLE

In-situ hydroxyapatite mineralization in beech and pine wood: effects of leaching on fire behavior

Matic Sitar[1,2] · Sabina Dolenec[1,3] · Nataša Knez[1] · Miha Hren[1] · Boštjan Lesar[2] · Andreja Pondelak[1]

Received: 10 December 2025 / Accepted: 16 March 2026

Abstract

This study presents the in-situ synthesis of hydroxyapatite (HAp) within the structure of beech and pine wood. The modification process utilized a two-step vacuum-pressure impregnation coupled with chemical precipitation using calcium nitrate tetrahydrate and diammonium hydrogen phosphate solutions, followed by exposure to ammonium hydroxide vapors. While the initial focus was on the overall physicochemical changes, microstructural characteristics and fire behavior of the mineralized wood, the main aim is to specifically investigate the effects of leaching. Because HAp synthesis produces water-soluble ammonium nitrate (NH_4NO_3) as a by-product, this research systematically addresses how the removal of this component affects the final properties of wood. HAp formation was confirmed by FTIR and X-ray diffraction, while scanning electron microscopy and microcomputed tomography revealed HAp deposits primarily in the cell lumen of both wood species. Fire behavior was evaluated using thermal analysis and the cone calorimeter. The incorporation of non-flammable HAp synthesized within the wood structure may act as a barrier and mass transfer during pyrolysis. This results to comparable or slightly enhanced key fire performance parameters when comparing leached HAp synthesized samples with leached reference samples. In contrast, the unleached HAp synthesized samples, which still contained residual NH_4NO_3, showed deterioration in fire growth rate (FIGRA) and heat release rate (HRR) parameters, confirming that NH_4NO_3 acts as an oxidant. However, this oxidative property also leads to improvements in total heat release (THR) and total smoke production (TSP) parameters compared to unleached references, representing a complex interaction when studying the fire properties of mineralized wood.

1 Introduction

As a natural hybrid composite material, wood is a versatile and widely used renewable resource for indoor and outdoor use (Teaca et al. 2019). However, wood's inherent susceptibility to fire, rapid heat spread and dense smoke production limit its wide applicability (Yu et al. 2024). These shortcomings of wood can be improved by incorporating flame retardant (FR) compounds. They inhibit the spread of fire and/or promote the formation of a protective char layer — especially in the case of phosphorus-based inhibitors. FRs can also remain on the wood surface and act as a physical barrier. Technological advances over the years have led to the development of various compounds, which are categorized as organic and inorganic. Among the organic FRs, nitrogen and phosphorus compounds are the most commonly used (Mensah et al. 2023). Phosphates function by oxidizing phosphorus to its most stable phase, beyond which no further oxidation can occur, making them inherently fire resistant (Toy and Walsh 1987). During the

✉ Andreja Pondelak
andreja.pondelak@zag.si

Matic Sitar
matic.sitar@zag.si

Sabina Dolenec
sabina.dolenec@zag.si

Nataša Knez
natasa.knez@zag.si

Miha Hren
miha.hren@zag.si

Boštjan Lesar
Bostjan.Lesar@bf.uni-lj.si

1 Slovenian National Building and Civil Engineering Institute, Dimičeva ulica 12, Ljubljana 1000, Slovenia

2 Biotechnical Faculty, University of Ljubljana, Jamnikarjeva 101, Ljubljana 1000, Slovenia

3 Faculty of Natural Sciences and Engineering, University of Ljubljana, Aškerčeva cesta 12, Ljubljana 1000, Slovenia

Published online: 15 April 2026

thermal decomposition of wood, these compounds promote dehydration reactions, which also lead to a reduction in the production of all volatiles (both combustible and non-combustible) (Levan 1984). However, most wood protection methods use harmful chemicals or processes, leading to environmental concerns. In particular, brominated flame retardants such as polybrominated diphenyl ethers (PBDEs), hexabromocyclododecane (HBCD), and tetrabromobisphenol A (TBBPA) are persistent and bioaccumulative compounds that have been detected in the environment and in humans, leading to increased regulatory scrutiny. Therefore, the development of sustainable and environmentally friendly wood modifications has recently taken center stage (Darnerud 2003; Dong et al. 2020; Feiteiro et al. 2021; Sandberg et al. 2017). One such solution is wood mineralization which generally refers to the integration of inorganic minerals, such as carbonates (Merk et al. 2015) and silicates (Mustoe 2023) into the wood structure.

One of the nature-inspired minerals that can be incorporated into wood is hydroxyapatite (HAp). HAp is the most common calcium phosphate, used in many fields of science, such as chemistry, biology and medicine (Dorozhkin 2009). Due to its high biocompatibility, strength and non-toxicity, it is widely used in biomedical applications, especially in orthopedics, dentistry, as well as a coating material for metal implants (Hendi 2017; Pu'ad et al. 2020). HAp has the chemical formula $Ca_{10}(PO_4)_6(OH)_2$ and is considered as poorly soluble in water and insoluble in alkaline solutions, but well soluble in acids. It is the second most stable and second least soluble calcium orthophosphate after fluorapatite (Dorozhkin 2009).

HAp can be synthesized using various techniques which can be divided into solid-state reactions and wet methods. The latter also includes chemical precipitation. This method is usually carried out under conditions of high pH, elevated temperature or both. If the synthesis conditions require lower pH values, the temperature should be increased and vice versa. Under such conditions, the formation of phase impurities (e.g. dibasic calcium phosphate anhydrate and octacalcium phosphate) is significantly reduced, which favors the formation of HAp (Catros et al. 2010; Ebrahimpour et al. 1993; Zhang and Lu 2007; Wang and Shaw 2007; Liu and Nancollas 1997). The formation of HAp by chemical precipitation is based on its low solubility and the high stability of the calcium phosphate phase in an aqueous environment at room temperature and pH values above 4 (Kim et al. 2010; Koutsopoulos et al. 2004; Zhang et al. 2003; Ikoma et al. 1999). However, the precipitation reaction is generally carried out at pH values above 4 and at temperatures from room temperature to near the boiling point of water (Catros et al. 2010; Ebrahimpour et al. 1993; Zhang and Lu 2008; Tao et al. 2007; Pang and Bao 2003; Lazic et al. 2001; Wang et al. 2005, 2006).

Hydrothermal synthesis is another wet method for the incorporation of HAp into wood, which works like a chemical precipitation process with an incubation stage conducted inside a pressure chamber (Zhang and Darvell 2010; Cihlar and Castkova 2002; Ioku et al. 2002; Yasukawa et al. 1999; Zhu et al. 2009; Manafi and Rahimipour 2011). The precursor solution usually contains a calcium and phosphate salt along with a pH adjusting agent such as ammonia or urea (Jokic et al. 2011). Nagata et al. (2013), for example, used a hydrothermal method with calcium nitrate tetrahydrate ($Ca(NO_3)_2{\cdot}4H_2O$) and diammonium hydrogen phosphate ($(NH_4)_2HPO_4$) for the successful synthesis of HAp.

Previous studies on fire-retardant mineralization employed thinner samples, such as the use of HAp in compressed bamboo veneers (100 mm × 100 mm × 6 mm) (He et al. 2024) or incorporated HAp nanosheets in porous balsam wood with dimensions of 10 mm × 50 mm × 4 mm (Xiao et al. 2024). Moreover, these studies do not address the potential impact of HAp synthesis by-products. Importantly, the fate of these reaction by-products after HAp synthesis is virtually undescribed, leaving their impact on the environment and fire behavior unknown. In contrast, Sitar et al. (2024) utilize Life Cycle Assessment (LCA) and Life Cycle Costing (LCC) to assess the potential negative environmental impacts of HAp mineralization, including process by-products, and compared them with commercial wood preparations in a practical example. When chemicals or energy-intensive processes are used, a longer life expectancy is necessary to justify the additional environmental impact. The main issue with the mineralization process was found to be water consumption during leaching.

This study reports in-situ hydroxyapatite (HAp) mineralization in beech and pine wood, focusing on how removing the water-soluble by-product ammonium nitrate (NH_4NO_3) affects the fire retardant properties of mineralized wood. The chemical, microstructural, and fire properties of unleached and leached modified wood samples were investigated. To our knowledge, this is the first study to systematically address the effects of leaching and the critical role of by-product formation during in-situ HAp synthesis in wood.

2 Materials and methods

2.1 Materials

Two common European wood species, beech (*Fagus sylvatica* L.) and pine sapwood (*Pinus sylvestris* L.) were included in the study using samples measuring 520 mm × 100 mm × 10 mm. Untreated beech samples had a density

Table 1 Leaching values of beech (B-Ref-L) and pine (P-Ref-L) reference samples as well as HAp synthesized beech (B-HAp-L) and pine (P-HAp-L) samples

Sample	Dry mass (g)	Dry mass- Impregnated (g)	Impregnated (%)	Dry mass-L (g)	Mass loss-L (%)	By-product loss-L (%)	HAp content (%)
B-Ref-L	297.8	-	-	295.0	0.9	-	-
P-Ref-L	307.6	-	-	305.3	0.7	-	-
B-HAp-L	307.5	374.1	21.7	328.2	14.0	64.5	7.7
P-HAp-L	300.9	374.4	24.4	327.7	14.8	60.7	9.6

of 672 kg/m^3 ± 26 kg/m^3, while untreated pine samples had a density of 533 kg/m^3 ± 28 kg/m^3. Before the mineralization process, the samples were conditioned at 23 °C ± 2 °C and 50% ± 5% relative humidity. The following chemicals were used for HAp synthesis: calcium nitrate tetrahydrate ($Ca(NO_3)_2 \cdot 4H_2O$), ammonium phosphate ($(NH_4)_2HPO_4$) and ammonium hydroxide solution (NH_4OH). Commercially available HAp (purity ≥ 90%) was also purchased to facilitate interpretation of the results. All chemicals were purchased from Sigma-Aldrich (USA), were of analytical grade and were used without further purification.

2.2 Methods

2.2.1 Mineralization process

The method of wood mineralization was adopted from Sitar et al. 2024. In short, the process focuses on forming HAp within the wood structure according to Eq. 1:

$$10Ca(NO_3) \cdot 4H_2O + 6(NH_4)_2HPO_4 + 8NH_4OH \rightarrow Ca_{10}(PO_4)_6(OH)_2 + 20NH_4NO_3 + 46H_2O \quad (1)$$

Beech and pine wood samples were impregnated using a two-step process in a vacuum-pressure chamber (VPT-135, Kambič, Slovenia). Two samples of each wood type were immersed in 1 M $Ca(NO_3)_2 \cdot 4H_2O$, and a 30-minute vacuum at 0.015 MPa was applied. While still immersed, the samples were then exposed to a pressure of 0.9 to 0.10 MPa for 6 h to ensure deeper penetration of $Ca(NO_3)_2 \cdot 4H_2O$ compounds into the wood. After the first impregnation process, the samples were removed from the solution, rinsed with deionized water, air-dried for 72 h, and oven-dried at 60 °C for 48 h to remove excess water. Next, the samples were immersed in 0.6 M $(NH_4)_2HPO_4$ and underwent a second 6-hour impregnation at 0.9 to 0.10 MPa in the vacuum-pressure chamber, this time without a vacuum step. After the second impregnation, the samples were exposed to NH_4OH solution vapors (NH_3 content of at least 25%) for 24 h at room temperature in a sealed box. The sealed box, without NH_4OH solution, was then placed in an oven at 80 °C for 24 h. This was followed by another 24-hour exposure to NH_4OH solution vapors and drying for 72 h at 80 °C, also in a sealed box. Finally, the impregnated samples were dried for 24 h in a chamber at 103 °C to reach dry mass. During synthesis, technological parameters such as mass uptake were measured. Prior to characterization, the mineralized samples were sawn to the dimensions required for further testing and stored at ambient conditions for at least seven days.

2.2.2 Characterization

The success of HAp mineralization was determined using various methods. FTIR spectroscopy (L1600400 Spectrum TWO, PerkinElmer, UK) and X-ray powder diffraction (XRD) were used to characterize the resulting products and the crystallinity of the mineral(s). FTIR spectra were recorded in ATR mode by placing a small amount of bulk sample directly on the ATR crystal and recorded in transmittance mode in the range 4000 to 400 cm^{-1} with a resolution of 4 cm^{-1}. Two measurements per sample were taken to ensure repeatability. XRD analyses were performed using a PANalytical Empyrean X-ray diffractometer (Malvern Panalytical, Malvern, UK) with CuKα radiation and a PIXcel 1D detector at 45 kV and a current of 40 mA in the range of 4 to 70° 2θ with a step size of 0.013° 2θ and a scan step time of 70 s. The samples were manually backloaded into a circular sample holder with a 10 mm diameter in order to mitigate the possible preferred orientation. The X-ray diffraction patterns were analyzed with PANalytical's X'Pert High Score Plus v. 4.9 diffraction software using PAN ICSD v. 3.4 powder diffraction files. For both methods, the HAp sample was scraped directly from the wood surface.

The leaching of active substances from wood was determined in accordance with standard SIST EN 84:2020. The proportion of losses of leached components was calculated according to Eq. 2:

$$\text{Mass loss} - \text{L}\ (\%) = \frac{(\text{Dry mass} - \text{Impregnated}\ (\text{g})) - (\text{Dry mass} - \text{L}\,(\text{g}))}{(\text{Dry mass} - \text{Impregnated}\ (\text{g}))} \times 100\% \quad (2)$$

where Dry mass-Impregnated (g) is starting dry mass of the sample after mineralization before the leaching process and Dry mass-L (g) is the mass after the leaching process.

The proportion of losses of mineralized components was calculated according to Eq. 3:

$$\text{By - product loss} - \text{L}\ (\%) = \frac{\text{Mass loss} - \text{L}\ (\%)}{((\text{Dry mass} - \text{Impregnated}\ (\text{g})) - (\text{Dry mass}\ (\text{g})))\,/\,(\text{Dry mass}\ (\text{g}))} \quad (3)$$

where Dry mass (g) is starting dry mass of the sample before the mineralization process.

Leaching was carried out with mineralized and reference beech and pine wood of the original dimensions. The comparison between leached and unleached samples was analyzed by FTIR, TG and cone calorimeter, while only leached samples were considered for microCT and SEM analysis.

MicroCT imaging was employed to investigate the distribution, position, size and quantity of HAp minerals in beech and pine wood. The EasyTom XL Ultra microCT system from RX Solutions (France) was used for this purpose. The microCT samples were prepared by cutting small rods (2 mm × 2 mm × 50 mm) from 520 mm × 100 mm × 10 mm samples. The wood region selected for microCT analysis was representative of the bulk material and was located approximately 1 cm from the sample edge and 3–5 mm beneath the surface. Imaging was performed using a Hamamatsu micro-focus X-ray source without filter, operated at a voltage of 40 kV, a tube current of 160 µA and a target anode current of 30 µA. A LaB6 filament was used as the cathode, which, according to the source manufacturer, guarantees a spatial resolution of at least 0.5 µm in small focus spot mode (SFC 0) at the given voltage. Radiographic images were captured with a high-speed flat-panel detector with a resolution of 2536 × 2024 pixels and a frame rate of 1 frame per second. A total of 3968 radiographs were captured during a full 360° rotation. Each radiograph was created by averaging five consecutive frames. The spatial resolution of the scans was 1.0 µm across the entire volume, achieved by positioning the samples at a source-to-object distance of 3.5 mm and a source-to-detector distance of 433 mm. Image reconstruction was performed using the integrated software from RX Solutions'. Only standard reconstruction parameters were used, such as center shift and source drift, which the RX Solutions' reconstruction software automatically imports and applies from the acquisition metadata. The reconstructed 3D volumes and cross-sectional slices were visualized and analysed using Dragonfly 3D visualization software (Comet Technologies Canada Inc.). HAp particles were binarized using visual interactive thresholding to determine the threshold value. Since HAp has approximately twice the density of the wood cell wall, the difference in image contrast caused by X-ray attenuation was used to distinguish HAp from the cell walls. Wood and HAp particles were then visualized together as two separate layers.

Scanning electron microscopy (SEM) (JEOL JSM-IT500, Oxford Instruments Analytical, USA) was used to determine the incorporation of HAp into the wood structure and the size and shape of the HAp particles formed. A high-vacuum mode with 20 kV electron acceleration, a working distance of 10 mm and a Backscattered electron detector were used. The SEM samples were cut out of a sample for microCT analysis using the ion-beam (approx. 2 mm × 2 mm × 5 mm).

The thermal behavior of the reference samples and the mineralized samples was characterized by thermal analysis (TG-DTA) (STA 409 Luxx, Netzsch, Germany). For analysis, the samples were cut in half, and the entire sawn surface was scraped. Approximately 50 mg of powder was used, and measurements were carried out in air atmosphere at a heating rate of 10 °C/min in the range of 25 °C to 1200 °C. Each sample category was tested three times to ensure repeatability.

Finally, the fire retardant behavior of the mineralized and reference samples was tested by cone calorimeter (Fire Testing Technology Instrument, UK). The samples were cut to the dimensions 100 mm x 100 mm x 10 mm and exposed to incident heat flux of 50 $kW \cdot m^{-2}$. Each test was carried out for 585 s and each sample category was tested five times to ensure reproducibility. Several parameters were calculated according to ISO 5660-1 (2015) and compared between the different sample categories. Some of the compared parameters were determined by observation, such as the time to ignition (TTI), defined as the time from the start of irradiation to steady flaming. A higher TTI value means later ignition and an improvement in certain fire characteristics. Some of the parameters are calculated from measured signals, e.g.

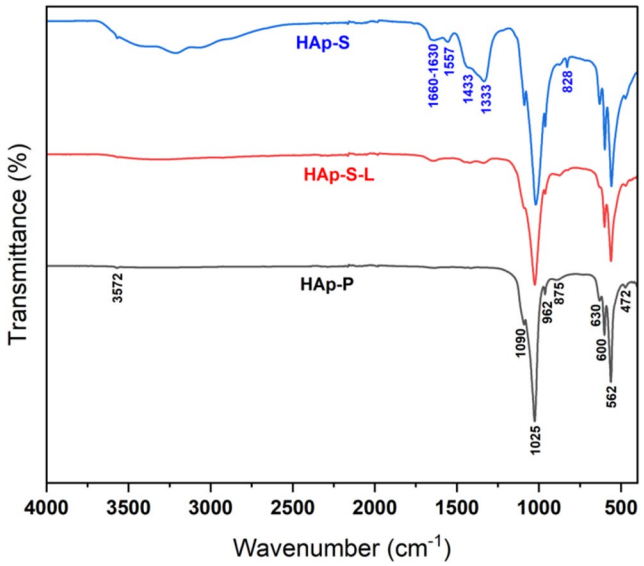

Fig. 1 FTIR spectra of unleached (HAp-S), leached (HAp-S-L) and purchased (HAp-P) HAp

the heat release rate (HRR) and its integral value, the total heat release (THR). Furthermore, measured data from cone calorimetry were used to estimate some of criteria parameters for reaction to fire classification, namely FIGRA (Fire Growth Rate Index) value. This parameter is typically calculated from SBI testing (EN 13823 (2022)), but for the purpose of this study, the simulation tool ConeTools (Van Hees et al. 2002) was used to predict the FIGRA value, which was one of the main parameters for determining the fire properties of the studied samples. For the measured parameters HRR, THR, total smoke production (TSP), and mean mass loss rate (MLR), higher values indicate poorer fire behavior. Similarly, a higher simulated FIGRA value reflects a faster increase in heat release, which also signifies poorer fire performance.

2.2.3 Data processing and analysis methods

Data were collected and processed using Microsoft Excel. Mean values and standard deviations were calculated from the data set and presented in graphs and tables. The number of samples studied for each material is specified for each method. Mass losses and mass uptakes were determined gravimetrically.

3 Results and discussion

3.1 Leaching process

The systematic leaching process, carried out in accordance with SIST EN 84:2020, was crucial for validating the flame retardancy of the HAp mineralization. As can be seen from Eq. 1, the synthesis of HAp produces NH_4NO_3 in addition to water. NH_4NO_3 is very soluble in water (i.e. 182 g/100 ml in H_2O (20 °C) (Trypuc and Druzynksi 2009), so that it can be easily removed from the wood by leaching. The amount of components leached from the wood is given in Table 1. It should be emphasized that the calculated values are not the main essence of this article, but the focus is on comparing the essential properties of leached and unleached mineralized samples. The weight% gain of impregnated compounds after mineralization in the beech wood sample (B-HAp-L) is 21.7% (Impregnated (%), while in pine wood it is 24.4% (P-HAp-L). Assuming that 0.9% of the wood compounds were leached out of the beech reference sample, the proportion of NH_4NO_3 is 14.0% (mass loss-L). This means that 64.5% (by-product loss-L) of the mineralized substances in the beech wood sample were removed during leaching. Assuming that 0.7% of the wood substances were leached from the pine reference sample, the NH_4NO_3 content is 14.8%. This means that 60.7% of the mineralized components were removed from the pine wood sample during leaching. However, the authors acknowledge that degradation processes caused by the treatment may contribute to higher leaching values compared to the untreated reference sample. Nevertheless, in Chap. 2.2.1, Mineralization Process, we describe the procedure in detail, noting that the use of elevated temperatures is adjusted to minimize damage to the wood while ensuring successful synthesis of HAp. The HAp content (%) in the B-HAp-L sample after the leaching process is 7.7%, while in the P-HAp-L sample it is 9.6%.

3.2 Characterization of HAp

The formation of HAp was investigated by FTIR studies. Figure 1 shows the FTIR spectra of HAp produced on wood (labelled HAp-S) and after leaching (labelled HAp-S-L). To facilitate interpretation, the FTIR spectra of purchased HAp are also shown (labelled HAp-P). As no significant differences were found between the wood species, only the results for HAp formed on beech wood are presented.

The most characteristic bands of synthesized HAp are PO_4^{3-}, OH^-, CO_3^{2-}, and HPO_4^{2-} (Berzina-Cimdina and Borodajenko 2012). The FTIR results of the purchased HAp show all bands characteristic for the analyzed compound. Impurities and by-products are not detectable. The PO_4^{3-} group is characterized by bands at 1090 cm^{-1}, 1025 cm^{-1}, 962 cm^{-1}, 600 cm^{-1}, 562 cm^{-1} and 472 cm^{-1}. The bands at 3572 cm^{-1} and 630 cm^{-1} belong to the OH^- group and are the most important FTIR bands of HAp, as they confirm its presence. The indistinct band at about 875 cm^{-1} could be attributed to both CO_3^{2-} and HPO_4^{2-}, as they are often difficult to separate at this value (Berzina-Cimdina and

Borodajenko 2012). It should be noted that not all commercially purchased HAp have the same properties such as degree of crystallinity and phase composition. A disadvantage of purchasing commercial calcium phosphate powders is the lack of sufficient information about the synthesis conditions and the raw materials used (Berzina-Cimdina and Borodajenko 2012).

In the synthesized HAp, both unleached and leached, all bands present in the purchased HAp can be observed. Unlike the purchased one, the unleached HAp shows additional bands. Weak bands between about 2600 cm^{-1} and 3600 cm^{-1} belong to OH^- and NH_4^+ groups. These two groups are also characterized by a weak band between 1630 cm^{-1} and 1660 cm^{-1}. The strong band at 1557 cm^{-1} is characteristic of the NH_4^+ group. The band at 1433 cm^{-1} is attributed to both the NO_3^- and NH_4^+ groups, while the strong bands at 1333 cm^{-1} and 828 cm^{-1} belong to the NO_3^- group. All the bands and groups mentioned are characteristic of the by-product of the synthesis – ammonium nitrate (NH_4NO_3), with the exception of the OH^- group, which represents absorbed water. However, most of these by-product bands are less pronounced or no longer recognizable in the FTIR spectra of the leached HAp sample (HAp-L), as NH_4NO_3 is highly soluble in water.

The XRD method provides information about the crystal structure of the material and its phase composition, but cannot be used to determine the presence of OH^- or CO_3^{2-} groups in HAp (Berzina-Cimdina and Borodajenko 2012). Figure 2 shows the results of the XRD analysis of purchased and synthesized HAp. As no significant differences were found in relation to leaching, only the results of the unleached samples are presented. There were also no differences between the wood species. The most characteristic diffraction peaks of HAp (JCPDS number [96-900-2215]), expressed in angles 2θ, are at 25.9 ° (002), 31.8 ° (211), 32.2 ° (112), 32.9 ° (300), 34.0 °(202), 39.8 ° (310), 46.7 ° (222), 49.5 ° (213) and 53.1 ° (004). All the above peaks confirm the successful synthesis of HAp in beech and pine wood. In contrast to the FTIR analysis, no by-products can be detected with the XRD method, as they are obviously not present in crystallized form.

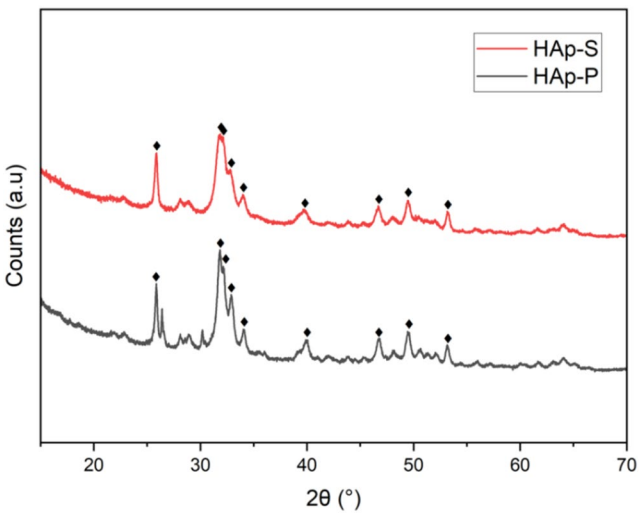

Fig. 2 XRD patterns of synthesized (HAp-S) and purchased (HAp-P) HAp

3.3 Characterization of mineralized wood

3.3.1 Micromorphological analysis

Figure 3a displays a cross-section of a mineralized beech wood, which shows that HAp is mainly deposited in the lumina of the cells, which are rarely completely filled. A radial cross-section of beech wood indicates that in some cases HAp is deposited over the entire length of the axial elements (Fig. 3b, marked with an arrow). Figure 3c shows a 3D representation of the scanned beech wood sample while Fig. 3d gives a 3D visualization of the deposition of HAp in the lumina of the beech.

The deposition of HAp in beech and pine wood was partly different. Figure 4a shows pine wood in which HAp is mainly found in the lumina of the tracheids, and in contrast to beech, HAp is also deposited along the rays (marked with an arrow). These results could be attributed to the higher porosity and longitudinal permeability of pine wood (Siau 1995). Figure 4b displays a radial section of pine wood, where HAp is also found in the parenchyma ray (marked with an arrow). Figure 4c shows a 3D representation of the scanned pine wood sample, while Fig. 4d gives a 3D visualization of the deposition of HAp in the pine wood. As reported by Merk et al. (2016), the pattern of mineral deposition in the wood appears to correspond to a microporous structure that facilitates the transport of the introduced compounds.

The mineralized wood was further evaluated by SEM analysis (Fig. 5). The cross-section of the beech wood confirmed that most HAp was deposited in the cell lumen (marked with a red arrow in Fig. 5a). In rare cases, HAp also fills wood pits (marked with a green arrow in Fig. 5a). In pine wood, HAp was also deposited in the luminal cells (marked with a red arrow in Fig. 5c) as well as in wood rays (marked with a blue arrow in Fig. 5c) and in some cases in wood pits (marked with a green arrow in Fig. 5c). The size of the HAp particles is between 2 µm and 10 µm (Figs. 5b and d). Based on the findings from the work of Sadat-Shojai et al. (2013), the HAp shown have a spherical shape (characteristic size range between 5 nm and 200 µm) and/or a flower-like shape (characteristic size range between 700 nm and 60 µm). Both shapes are considered to be produced by chemical precipitation and hydrothermal method.

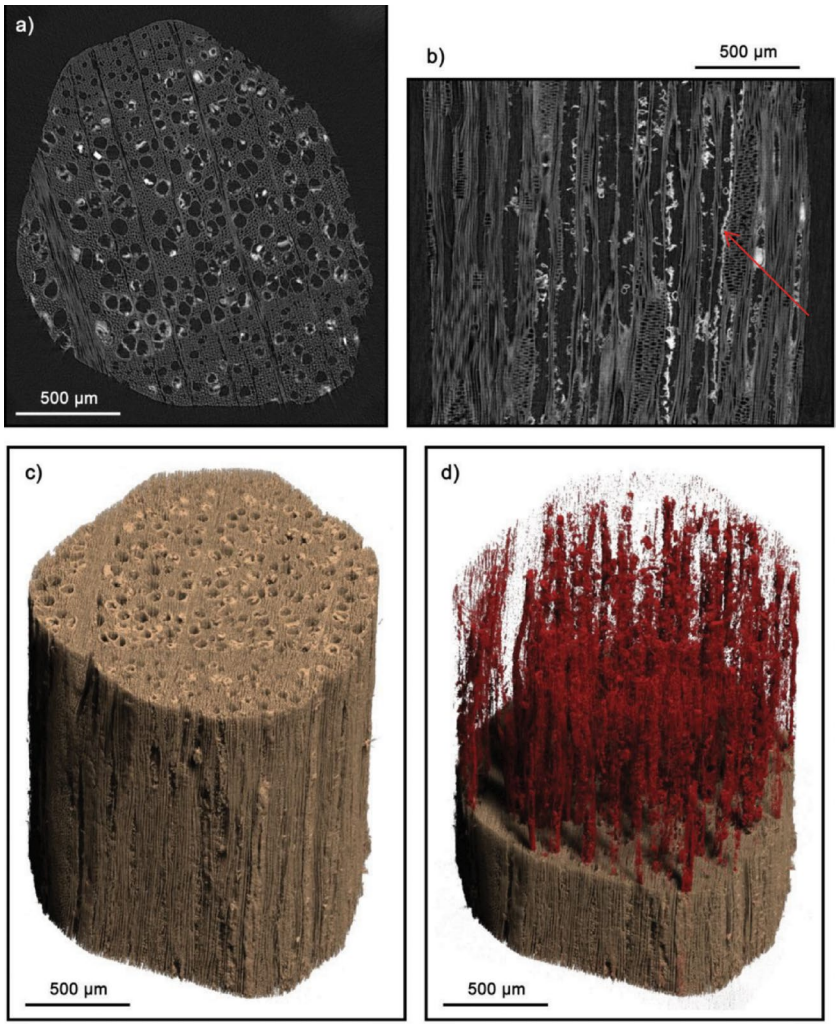

Fig. 3 MicroCT scan of a beech wood sample mineralized with HAp: characteristic **a** axial and **b** radial cross-section, 3D representation of the entire scanned volume (**c**) and of the same volume with HAp particles shown in red (**d**)

3.3.2 Thermal properties

TG and DTG were used to assess thermal stability and the degradation process of mineralized wood. Figure 6a and c show the TG curves of reference and mineralized beech and pine wood samples. Since the reference samples showed no differences after leaching, only the unleached samples are presented. Figure 6b and d show the curves of the normalized weight loss rates of the samples.

While three main regions of weight loss were identified across all samples, the unleached mineralized sample show a fourth decomposition stage linked to the thermal breakdown of a by-product. The first region lasts until 150 °C and the weight loss is up to 10% with peaks between 115 °C and 120 °C. The mass loss in the first region is due to the evaporation of surface-bound water (Garskaite et al. 2023). The second major degradation occurs from 200 °C to 400 °C. This stage exhibits the highest weight loss (between 45% and 55%), with HAp content being the determining factor for the final value. The second region is characterized primarily by the breakdown of complex carbohydrates, starting with hemicelluloses at around 200 °C. This process results in the release of CO and CO_2 as major components along with minor components such as H_2, CH_4, C_2H_4 and H_2O. The thermal decomposition of cellulose takes place at higher temperatures (315 °C to 400 °C), with the main maximum in the weight loss rate between 325 °C and 350 °C. Hemicellulose has an amorphous structure, whereas cellulose is a semi-crystalline polymer, which leads to its greater thermal stability (Chen et al. 2014; Nurazzi et al. 2021; Chaturvedi and Dave 2013). B-Ref exhibits an additional DTG peak around 290 °C, separated from the main cellulose peak, which is characteristic of acetylated hemicelluloses decomposition typical in hardwoods. P-Ref, however, presents a smoother transition, a result of the overlapping degradation of its extractives and hemicellulose components. Consequently, the clear secondary peak near 300 °C is characteristic for hardwood species with lower extractive content and higher hemicellulose proportion (Poletto et al. 2012; Yang et al. 2007; Chen et al. 2014; Nurazzi et al. 2021). The third

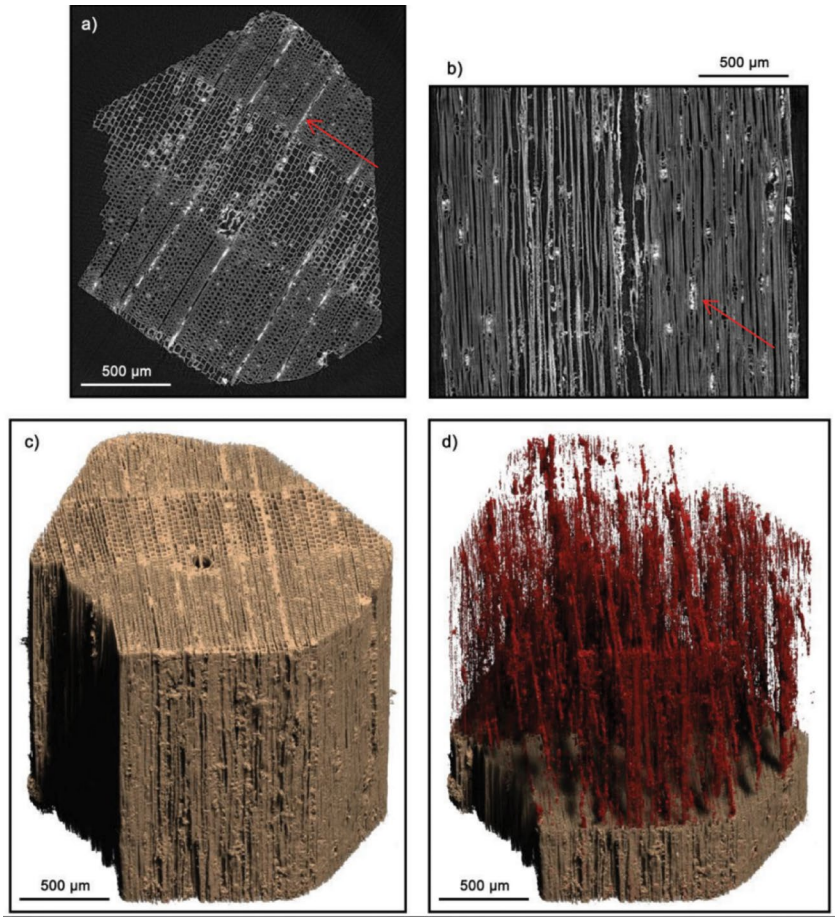

Fig. 4 MicroCT scan of a pine wood sample mineralized with HAp: characteristic **a** axial and **b** radial cross-section, 3D representation of the entire scanned volume (**c**) and of the same volume with HAp particles shown in red (**d**)

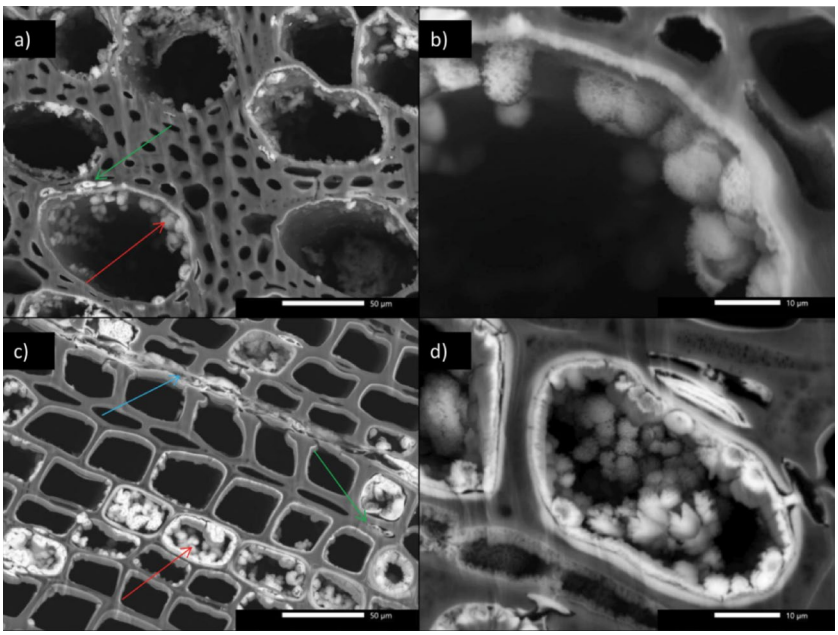

Fig. 5 SEM images of synthesized HAp in beech (**a**, **b**) and pine wood (**c**, **d**)

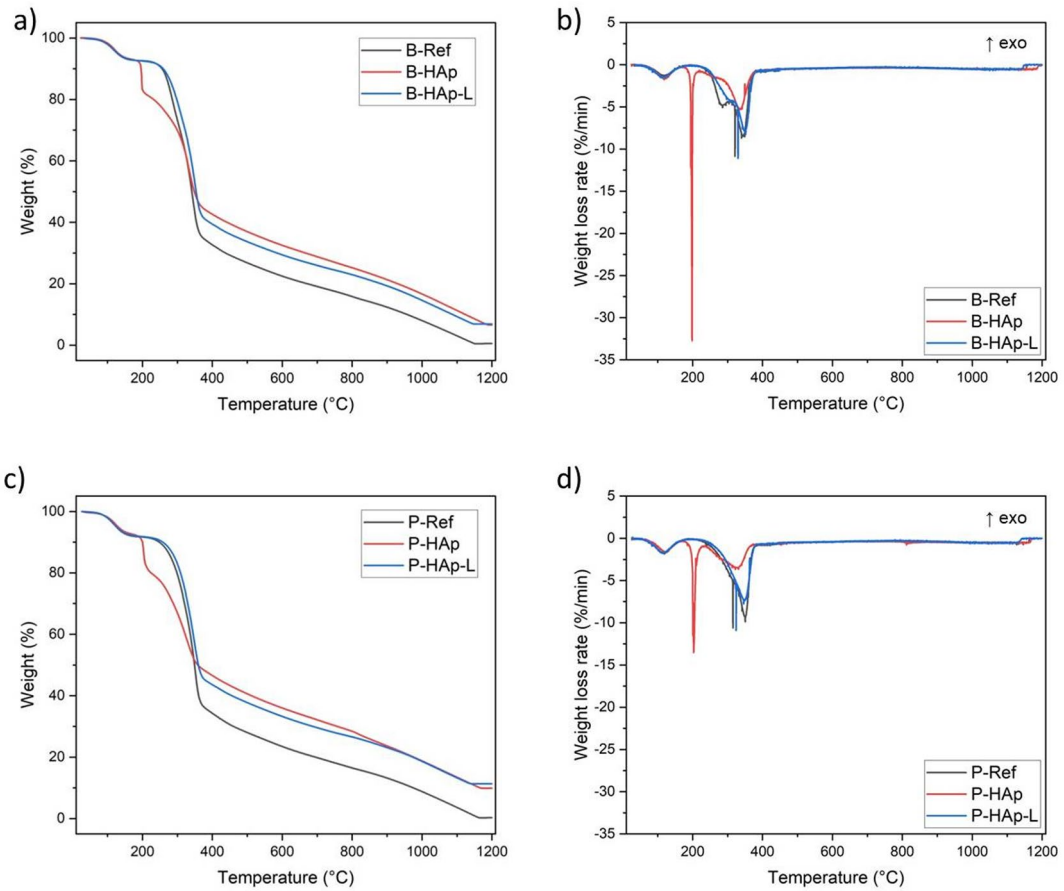

Fig. 6 TG curves of **a** beech wood (B-Ref, B-HAp and B-HAp-L) and **c** pine wood (P-Ref, P-HAp and P-HAp-L) samples, as well as their DTG values: **b** beech and **d** pine samples

region is associated with lignin degradation and calcination phase. The lignin degrades slowly and over a wider temperature range (from 150 °C to 900 °C) (Yang et al. 2007). The unleached HAp curves exhibit a distinct shape compared the other four. Specifically, the unleached mineralized samples (red curves) show a pronounced 10% mass loss and accelerated combustion at approximately 200 °C. This thermal event directly corresponds to the known decomposition temperature of the residual NH_4NO_3 (Chaturvedi and Dave 2013), chemically validating the removal goal of the leaching procedure. The B-HAp sample exhibits a significantly higher intensity for this low-temperature peak compared to P-HAp. This suggest that denser structure and higher ion-binding capacity of the beech wood enhance the retention of NH_4^+/NO_3^- ions within the cell wall, leading to a stronger and more pronounced DTG signal during their localized degradation (Chaturvedi and Dave 2013; Siau 1984; Hill 2006). The temperature regions above 400 °C represents the final calcination phase consists a remaining weight loss of approximately 35%. The curves in this region are flatter, indicating the gradual degradation of the residual charcoal (Catros et al. 2010; Sadat-Shojai et al. 2013; Garskaite et al. 2023) and HAp residue.

We observe no thermal decomposition for HAp within the measured temperature range, which is reflected in decreased weight loss after heating to 1200 °C. This results is consistent with findings by Liao et al. (1999) who state that the release of OH^- ions from HAp begins between 1000 °C and 1360 °C and the onset of HAp degradation is not typically detected below 1350 °C. Given that our maximum experimental temperature was 1200 °C, complete decomposition of HAp was not expected. This was also confirmed by FTIR analysis (Fig. S1). The leaching process changes the TGA curve`s shape but does not affect the final mass loss percentage. Studies of wood mineralization with calcium phosphates or HAp report slower weight loss during heating, reduced exothermic peaks, and increased char residue, suggesting that the incorporated HAp acts as a thermal barrier phase and also reduces the rate of degradation of cellulose, lignin and hemicelluloses (Akaki et al. 2012; Yang et al. 2024; Guo et al. 2018). All samples modified with HAp show greater thermal stability compared to the references. The DTG peaks for the mineralized wood are, particularly

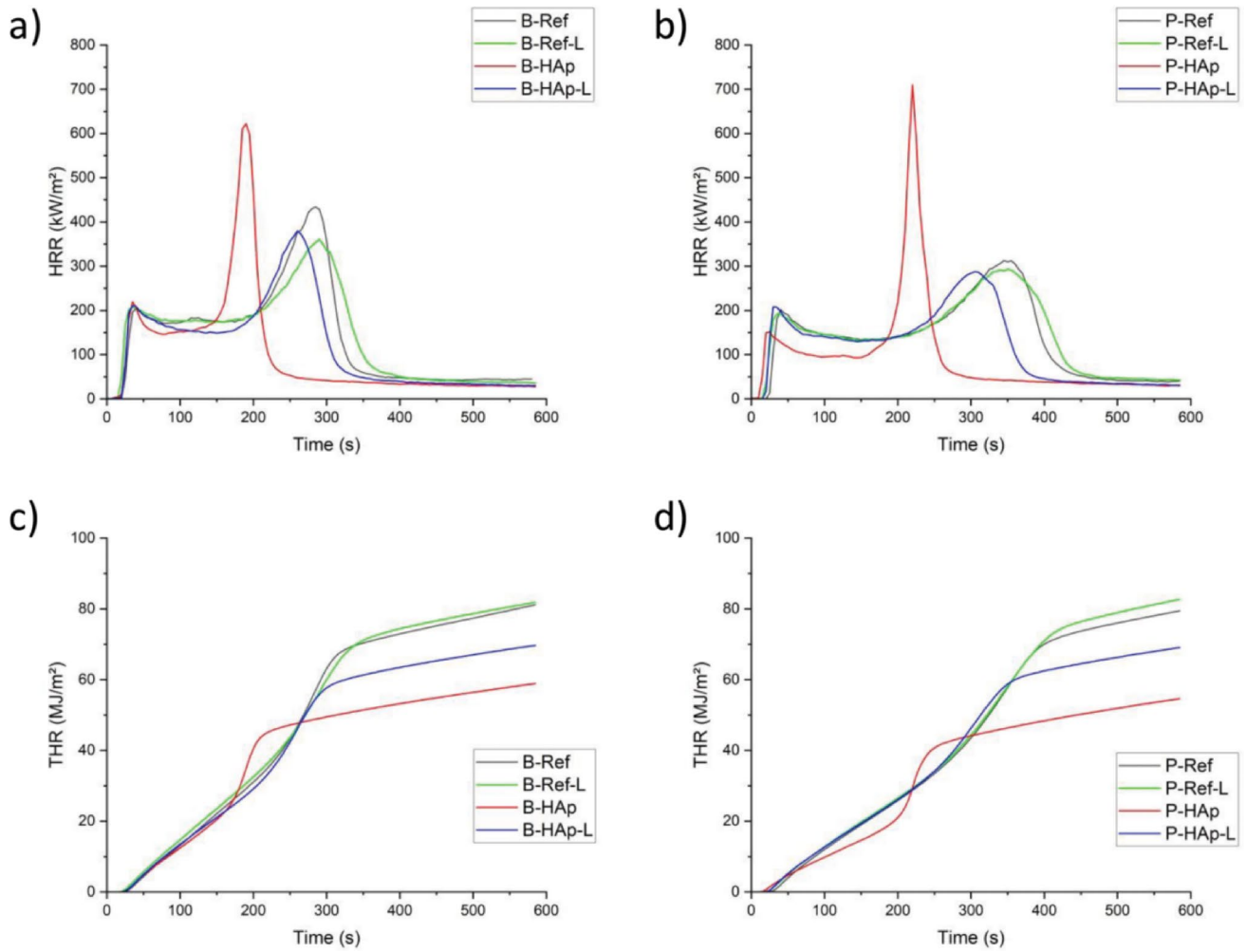

Fig. 7 Cone calorimeter curves of heat release rate (**a**, **b**) and total heat release **(c**,**d)** for beech wood (B-Ref, B-Ref-L, B-HAp and B-HAp-L) (**a**, **c**) and pine wood (P-Ref, P-Ref-L, P-HAp and P-HAp-L) **(b**, **d)** samples. Each curve shows the average of five measurements

Table 2 TTI, FIGRA, TSP and mean MLR values for reference samples of beech (B-Ref) and pine (P-Ref) wood, HAp synthesized beech (B-HAp) and pine (P-HAp) wood samples and the corresponding leached counterparts (B-Ref-L, B-HAp-L, P-Ref-L and P-HAp-L)

Sample	TTI (s)	FIGRA [W/s]	TSP [m^2]	mean MLR [g/s]
B-Ref	29.5±3.7	525.6±57.2	2.4±0.1	0.092±0.002
B-Ref-L	23.4±2.2	687.3±73.5	3.2±0.2	0.059±0.006
B-HAp	29.2±4.4	587.1±77.6	1.1±0.1	0.070±0.008
B-HAp-L	27.2±2.0	544.8±51.8	3.3±0.3	0.066±0.015
P-Ref	31.2±3.0	422.9±45.8	3.7±0.2	0.091±0.001
P-Ref-L	24.6±3.4	558.4±77.1	4.8±0.2	0.060±0.010
P-HAp	20.0±2.3	492.2±31.4	1.1±0.2	0.068±0.009
P-HAp-L	26.4±3.3	508.1±79.8	4.5±0.2	0.066±0.008

in the second region, lower compared to the reference samples, which indicates a slower degradation rate of wood distributed over a wider temperature range. Leaching further improves thermal stability by removing NH_4NO_3, as indicated by the absence of low-temperature DTG signals.

3.3.3 Fire retardant behavior

Cone calorimetry was used to evaluate the fire retardant properties of mineralized wood (Fig. 7; Table 2). The enhanced fire retardancy of HAp in cellulose-based nanocomposite and bamboo has already been described by Xiao et al. (2024) and He et al. (2024), respectively. Therefore, the proposed study not only focuses on the fire performance of mineralized wood, but also thoroughly evaluates the effects of leaching HAp synthesis by-products (i.e., NH_4NO_3) from wood.

The results for the TTI parameter among the studied materials do not show significant differences, either between the synthesized HAp and the reference samples or between the two wood species. The observed differences between the samples are generally minimal and may be influenced by both the variability of the wood and the variability of the TTI parameter in cone calorimeter testing. The FIGRA values are higher for beech wood than for pine wood samples

because wood with higher cellulose and lower resin content (such as beech) releases more heat than wood with lower cellulose and higher resin content (such as pine) (Demirbas 2002). Additionally, beech wood typically has a much higher density than pine, which significantly affects heat release and related fire parameters such as FIGRA (Zhou et al. 2024). Both mineralized unleached wood species have a higher FIGRA value compared to the unleached references. B-HAp shows an increase of 11.7%, while B-HAp-L decreases by 20.7% compared to the reference values. In the case of pine wood, the FIGRA value for P-HAp increased by 16.4% and decreased by 9.0% for P-HAp-L compared to the reference values. By determining the thermal properties, it was demonstrated that NH_4NO_3 in unleached samples thermally decomposes at temperatures around 200 °C, causing accelerated combustion and confirming that NH_4NO_3 acts as an oxidizing agent (Chaturvedi and Dave 2013). Despite the small number of samples and the well-known high variability of FIGRA values, the results showed that the oxidizing role of NH_4NO_3 directly leads to accelerated and increased heat release, which increases the FIGRA value of unleached mineralized samples. Classical phosphorus inhibitors (e.g., ammonium polyphosphate) release acids that strongly dehydrate cellulose and accelerate charring. HAp, on the other hand, acts as a barrier, an indirect charring catalyst, and a VOC adsorbent without releasing free acids (Velencoso et al. 2018; Ozyhar et al. 2022).

The TSP values at 585 s are between 2.4 m^2 and 3.2 m^2 (beech wood) and between 3.7 m^2 and 4.8 m^2 (pine wood) for the reference samples. Higher TSP values in pine wood samples could be attributed to a higher lignin (Lourenço and Pereira 2018) and resin content (Frodeson et al. 2021). Both mineralized samples show a reduction in TSP values (54.2% for B-HAp and 70.3% for P-HAp) compared to the unleached reference samples. The leaching of the mineralized samples increases the TSP content compared to the leached reference samples. In contrast to previous findings, the unleached samples produce significantly less TSP than the leached samples. The TSP analysis revealed a complex counter-effect: the more flammable, NH_4NO_3-loaded unleached samples showed significantly lower smoke production compared to the references. This counterintuitive result is attributed to the presence of the oxidizing agent NH_4NO_3, which promotes more complete combustion and thus reduces the formation of soot and particulate matter (Chaturvedi and Dave 2013), and illustrates the unique chemical interactions in this specific synthesis pathway. HAp can also adsorb or catalytically decompose some organic vapors produced during wood pyrolysis. As a result, the amount of combustible gases around the material is reduced, contributing to decreased flame spread (Guo et al. 2018; Xin et al. 2020). This complex interplay between the oxidant by-product, increased heat release (FIGRA) and reduced smoke (TSP) is a new finding specific to this HAp synthesis method. When examining the mean MLR values in this study, no significant influence of wood species was observed within the experimental variability, as similar trends were found for both beech and pine. The highest values were recorded for the unleached reference samples (B-Ref and P-Ref). The leached samples showed slightly lower mean MLR values, which may be attributed to the removal of water-soluble extractives and low-molecular-weight compounds that contribute to fuel generation during thermal decomposition (White and Dietenberger 2010). Additionally, the lower mean MLR values of B-HAp and P-HAp compared to the references indicate that the introduction of HAp may act as a barrier to heat and mass transfer during pyrolysis, thereby slowing the release of combustible volatiles (Lowden and Hull 2013; Babrauskas 2002).

Figures 7a and b show that all samples exhibit a bimodal curve, with the first HRR peak occurring immediately after ignition, before a protective char forms on the surface. As combustion proceeds, the HRR curve decreases, indicates the formation of protective char. The second, higher peak is caused by the formation of cracks in the charcoal when the heat wave reaches the last insulating surface and the heat accumulates in the thermally insulating kaowool, while the original material has already been heated to pyrolysis temperature (Schartel and Hull 2007; Schartel et al. 2005; Batiot et al. 2014; Yi et al. 2024). For the two mineralized unleached samples (red curves in Fig. 7a and b), the maximum heat release occurs significantly faster (B-HAp at 190 s and P-HAp at 220 s) than for all other samples. They also show higher values (190 kW/m^2 more for B-HAp and 400 kW/m^2 more for P-HAp) compared to the unleached reference samples. The higher HRR of the unleached mineralized samples can be attributed to the combustion of NH_4NO_3, which is reflected in the high but narrow peak. However, it should be emphasized that the shape of the narrow peak leads to lower THR values (as described in the next section). In the HAp leached samples, the higher HRR peak appears earlier (30 s earlier for B-HAp-L and 40 s earlier for P-HAp-L) than in the leached reference samples. However, both peaks show approximately the same HRR values (kW/m^2) as the reference samples. The results showed that the effect of HAp on the HRR parameter is less pronounced than that of other phosphorus flame retardants.

The THR values (Figs. 7c and d) at 585 s are between 79 and 82 MJ/m^2 for all reference samples. Mineralized beech wood samples exhibited a reduction of 27.4% (B-HAp) and 14.9% (B-HAp-L), while mineralized pine wood samples showed a reduction of 31.3% (P-HAp) and 16.4% (P-HAp-L) compared to the reference and reference leached samples. The B-HAp curve shows a steep increase between 150 s

and 200 s when NH_4NO_3 is released. From 250 s onwards, the value is the lowest among all beech wood samples. A similar trend applies to P-HAp, with the difference that the steep increase occurs about 50 s later. It can be seen that despite the described sharp increase in THR values when NH_4NO_3 is released, this has no influence on the final THR values. The contribution of the mineral as a flame retardant might be in the condensed phase that is evidenced by the lower THR values in all mineralized samples (leached and unleached) compared to the reference samples. This confirms that the non-combustible HAp incorporated in the wood structure acts as a barrier for heat and mass transfer during pyrolysis (Merk et al. 2016). Once the accelerating effect of NH_4NO_3 is removed, HAp promotes the formation of a stable char layer that protects the lower layers of wood from oxygen and further combustion. Although HAp is not a strong dehydration catalyst like ammonium polyphosphate, the surface PO_4^{3-} groups and Ca^{2+} centers promote polysaccharide condensation and char formation (Akaki et al. 2012; Velencoso et al. 2018; Ozyhar et al. 2022), which is reflected in a flatter THR curve and the lowest final THR values in all categories.

4 Conclusions

This study successfully demonstrated the synthesis of hydroxyapatite (HAp) in-situ in both beech and pine via chemical precipitation, resulting in the deposition of spherical and/or flower-like particles predominantly in the cell lumen and rays. The fire performance analysis provided crucial mechanistic insight, focusing on the synthesis by-product ammonium nitrate (NH_4NO_3). It was confirmed that NH_4NO_3 acts as an oxidant, causing deterioration of FIGRA and HRR parameters in unleached HAp synthesized samples. On the other hand, the unleached samples showed improvements in THR and TSP values compared to unleached references. The deterioration of two parameters and the simultaneous improvement of two others, caused by the by-product formed during HAp synthesis within the wood structure, represent a complex interaction specific to this method of HAp incorporation. Leached HAp synthesized samples, without NH_4NO_3, do not show significant differences compared to leached references for most of the studied parameters. The presence of non-combustible HAp embedded in the wood structure may, to some extent, act as a barrier to heat and mass transfer during pyrolysis. Although HAp is not a strong dehydration catalyst, the surface PO_4^{3-} groups and Ca^{2+} centers promote polysaccharide condensation and char formation. This study provides significant insight into the HAp mineralization process, highlighting the critical relationship between the water-soluble NH_4NO_3 synthesis by-product and its profound effect on material fire performance. This work establishes guidelines for the future application of bio-inspired phosphate mineralization processes in green building materials.

Supplementary Information The online version contains supplementary material available at https://doi.org/10.1007/s00107-026-02412-6.

Acknowledgements This research was funded by the Slovenian Research and Innovation Agency (ARIS), within the research core funding's P4-0430, P2-0273, and P4-0015 and research project J7-50231.

Author contributions M. S.: Conceptualization, Investigation, Data curation, Visualization, Writing – original draft, Writing – review & editing. S. D.: Investigation, Writing – review & editing. N. K.: Investigation, Writing – review & editing. M. H.: Investigation, Visualization Writing – review & editing. B. L.: Supervision, Conceptualization, Data curation, Writing – review & editing. A. P.: Supervision, Conceptualization, Investigation, Data curation, Writing – review & editing, Funding acquisition. All authors reviewed the manuscript.

Data availability No datasets were generated or analysed during the current study.

Declarations

Conflict of interest The authors declare no competing interests.

References

Akaki T, Maehara H, Tooyama M (2012) Development of wood and wood ash-based hydroxyapatite composites and their fire-retarding properties. J Wood Sci 58(6):532–537. https://doi.org/10.1007/s10086-012-1276-4

Babrauskas V (2002) The cone calorimeter. In P. J. DiNenno (Ed.), SFPE handbook of fire protection engineering (3rd ed.). National Fire Protection Association. https://doi.org/10.1007/978-1-4939-2565-0

Batiot B, Luche J, Rogaume T (2014) Thermal and chemical analysis of flammability and combustibility of fir wood in cone calorimeter coupled to FTIR apparatus. Fire Mater 38(3):418–431. https://doi.org/10.1002/fam.2192

Berzina-Cimdina L, Borodajenko N (2012) Research of calcium phosphates using Fourier transform infrared spectroscopy. In: Infrared

spectroscopy – materials science, engineering and technology. https://doi.org/10.5772/36942
Catros S, Guillemot F, Lebraud E, Chanseau C, Perez S, Bareille R, Amédée J, Fricain JC (2010) Physico-chemical and biological properties of a nano-hydroxyapatite powder synthesized at room temperature. IRBM 31(4):226–233. https://doi.org/10.1016/j.irbm.2010.04.002
Chaturvedi S, Dave P (2013) Review on thermal decomposition of ammonium nitrate. J Energetic Mater 31(1):1–26. https://doi.org/10.1080/07370652.2011.573523
Chen Y, Tshabalala MA, Gao J, Stark NM, Fan Y, Ibach RE (2014) Thermal behavior of extracted and delignified pine wood flour. 591:40–44. https://doi.org/10.1016/j.tca.2014.06.012
Cihlar J, Castkova K (2002) Direct synthesis of nanocrystalline hydroxyapatite by hydrothermal hydrolysis of alkylphosphates. Monatsh Chem 133(6):761–771
Darnerud PO (2003) Toxic effects of brominated flame retardants in man and in wildlife. Environ Int 29(6):841–853. https://doi.org/10.1016/S0160-4120(03)00107-7
Demirbas A (2002) Relationships between heating value and lignin, moisture, ash and extractive contents of biomass fuels. Energy Explor Exploit 20(1):105–111. https://doi.org/10.1260/0144598027601704 20
Dong Y, Wang K, Li J, Zhang S, Shi SQ (2020) Environmentally benign wood modifications: a review. ACS Sustainable Chem Eng 8(9):3532–3540. https://doi.org/10.1021/acssuschemeng.0c00342
Dorozhkin SV (2009) Calcium orthophosphates in nature, biology and medicine. Materials 2:399–498. https://doi.org/http://dx.doi. https://doi.org/10.3390/ma2020399
Ebrahimpour A, Johnsson M, Richardson C, Nancollas G (1993) The characterization of hydroxyapatite preparations. J Colloid Interface Sci 159(1):158–163
European Committee for Standardization (2022) EN 13823:2020+A1:2022 Reaction to fire tests for building products – Building products excluding floorings exposed to the thermal attack by a single burning item. CEN, Brussels
Feiteiro J, Mariana M, Cairrão E (2021) Health toxicity effects of brominated flame retardants: From environmental to human exposure. Environ Pollut 285:117475. https://doi.org/10.1016/j.envpol.2021.117475
Frodeson S, Anukam A, Berghel J, Ståhl M, Nilsson R, Henriksson G, Aladejana E (2021) Densification of wood - influence on mechanical and chemical properties when 11 naturally occurring substances in wood are mixed with beech and pine. Energies 14(18). https://doi.org/10.3390/en14185895
Garskaite E, Balciunas G, Drienovsky M, Sokol D, Sandberg D, Bastos A, Salak A (2023) Brushite mineralised Scots pine (Pinus sylvestris L.) sapwood - revealing mineral crystallization within a wood matrix by in situ XRD. RSC Adv 13(9):5813–5825. https://doi.org/10.1039/d3ra00305a
Guo W, Wang X, Zhang P, Liu J, Song L, Hu Y (2018) Nano-fibrillated cellulose-hydroxyapatite based composite foams with excellent fire resistance. Carbohydr Polym 195:71–78. https://doi.org/10.1016/j.carbpol.2018.04.063
He L, Bao G, Yu X, Zhang X, Jin X, Yu Z, He Y, Zhang R, Qin D (2024) A green and eco-friendly method to enhance Bamboo flame resistance via calcium alginate assisted in-situ mineralization of hydroxyapatite. Chem Eng J 485. https://doi.org/10.1016/j.cej.2024.149765
Hendi AA (2017) Hydroxyapatite based nanocomposite ceramics. J Alloys Compd 712:147–151. https://doi.org/10.1016/j.jallcom.2017.04.021
Hill CAS (2006) Wood modification: chemical, thermal and other processes. Wiley, Chichester
Ikoma T, Yamazaki A, Nakamura S, Akao M (1999) Preparation and structure refinement of monoclinic hydroxyapatite. J Solid State Chem 144(2):272–276
International Organization for Standardization (2015) ISO 5660-1:2015 Reaction-to-fire tests — Heat release rate (cone calorimeter method) and smoke production rate (dynamic measurement). ISO, Geneva
Ioku K, Yamauchi S, Fujimori H, Goto S, Yoshimura M (2002) Hydrothermal preparation of fibrous apatite and apatite sheet. Solid State Ion 151(1–4):147–150
Jokic B, Mitric M, Radmilovic V, Drmanic S, Petrovic R, Janackovic D (2011) Synthesis and characterization of monetite and hydroxyapatite whiskers obtained by a hydrothermal method. Ceram Int 37(1):167–173. https://doi.org/10.1016/j.ceramint.2010.08.032
Kim D, Cho I, Kim J, Jang H, Han G, Ryu H, Shin H, Jung H, Kim H, Hong K (2010) Simple large-scale synthesis of hydroxyapatite nanoparticles: In situ observation of crystallization process. Langmuir 26(1):384–388. https://doi.org/10.1021/la902157z
Koutsopoulos S, Barlos K, Gatos D, Dalas E (2004) The effect of various Prothymosin α fragments on the crystal growth of hydroxyapatite in aqueous solution. J Cryst Growth 267(1–2):306–311. https://doi.org/10.1016/j.jcrysgro.2004.03.054
Lazic S, Zec S, Miljevic N, Milonjic S (2001) The effect of temperature on the properties of hydroxyapatite precipitated from calcium hydroxide and phosphoric acid. Thermochim Acta 374(1):13–22
Levan SL (1984) Chemistry of fire retardancy. Adv Chem Ser 207:531–574
Liao CJ, Lin FH, Chen KS, Sun JS (1999) Thermal decomposition and reconstitution of hydroxyapatite in air atmosphere. Biomaterials 20(19):1807–1813. https://doi.org/10.1016/s0142-9612(99)00076-9
Liu Y, Nancollas G (1997) Crystallization and colloidal stability of calcium phosphate phases. J Phys Chem B 101(18):3464–3468
Lourenço A, Pereira H (2018) Compositional variability of lignin in biomass. In: Lignin - Trends and Applications. https://doi.org/10.5772/intechopen.71208
Lowden LA, Hull TR (2013) Flammability behaviour of wood and a review of the methods for its reduction. Fire Sci Rev 2(4). https://doi.org/10.1186/2193-0414-2-4
Manafi S, Rahimipour M (2011) Synthesis of nanocrystalline hydroxyapatite nanorods via hydrothermal conditions. Chem Eng Technol 34(6):972–976. https://doi.org/10.1002/ceat.201000393
Mensah R, Jiang L, Renner J, Xu Q (2023) Characterisation of the fire behaviour of wood: from pyrolysis to fire retardant mechanisms. J Therm Anal Calorim 148(4):1407–1422. https://doi.org/10.1007/s10973-022-11442-0
Merk V, Chanana M, Keplinger T, Gaan S, Burgert I (2015) Hybrid wood materials with improved fire retardance by bio-inspired mineralisation on the nano- and submicron level. Green Chem 17(3):1423–1428. https://doi.org/10.1039/c4gc01862a
Merk V, Chanana M, Gaan S, Burgert I (2016) Mineralization of wood by calcium carbonate insertion for improved flame retardancy. Holzforschung 70(9):867–876. https://doi.org/10.1515/hf-2015-0228
Mustoe G (2023) Silicification of wood: An overview. Minerals 13. https://doi.org/10.3390/min13020206
Nagata F, Yamauchi Y, Tomita M, Kato K (2013) Hydrothermal synthesis of hydroxyapatite nanoparticles and their protein adsorption behavior. J Ceram Soc Jpn 121(1417):797–801. https://doi.org/10.2109/jcersj2.121.797
Nurazzi N, Asyraf M, Rayung M, Norrrahim M, Shazleen S, Rani M, Shafi A, Aisyah H, Radzi M, Sabaruddin F, Ilyas R, Zainudin E, Abdan K (2021) Thermogravimetric analysis properties of cellulosic natural fiber polymer composites: A review on influence of chemical treatments. Polymers 13(16). https://doi.org/10.3390/polym13162710

Ozyhar T, Tschannen C, Thoemen H, Zoppe J (2022) Evaluating the use of calcium hydrogen phosphate dihydrate as a mineral-based fire retardant for application in melamine-urea-formaldehyde (MUF)-bonded wood-based composite materials. Fire Mater 46(3):595–604. https://doi.org/10.1002/fam.3009

Pang Y, Bao X (2003) Influence of temperature, ripening time and calcination on the morphology and crystallinity of hydroxyapatite nanoparticles. J Eur Ceram Soc 23(10):1697–1704

Poletto M, Zattera A, Santana R (2012) Thermal decomposition of wood: Kinetics and degradation mechanisms. Bioresour Technol 126:7–12. https://doi.org/10.1016/j.biortech.2012.08.133

Pu'ad N, Haq RHA, Noh HM, Abdullah HZ, Idris MI, Lee TC (2020) Synthesis method of hydroxyapatite: A review. Today Proc 29:233–239. https://doi.org/10.1016/j.matpr.2020.05.536

Sadat-Shojai M, Khorasani MT, Dinpanah-Khoshdargi E, Jamshidi A (2013) Synthesis methods for nanosized hydroxyapatite with diverse structures. Acta Biomater 9(8):7591–7621. https://doi.org/10.1016/j.actbio.2013.04.012

Sandberg D, Kutnar A, Mantanis G (2017) Wood modification technologies - a review. IFOREST 10:895–908. https://doi.org/10.3832/ifor2380-010

Schartel B, Hull T (2007) Development of fire-retarded materials - Interpretation of cone calorimeter data. Fire Mater 31(5):327–354. https://doi.org/10.1002/fam.949

Schartel B, Bartholmai M, Knoll U (2005) Some comments on the use of cone calorimeter data. Polym Degrad Stab 88(3):540–547. https://doi.org/10.1016/j.polymdegradstab.2004.12.016

Siau JF (1984) Transport processes in wood. Springer-, Berlin

Siau JF (1995) Wood: influence of moisture on physical properties. Virginia Poly Institute and State University, Blacksburg

Sitar M, Kuzman M, Oblak L, Remic K (2024) Environmental and economic impacts of hydroxyapatite mineralized wood: LCA and LCC analysis. Forests 15(9). https://doi.org/10.3390/f15091532

Slovenian Institute for Standardization (2020) SIST EN 84:2020 Durability of wood and wood-based products - Accelerated ageing of treated wood prior to biological testing - Leaching procedure. SIST, Ljubljana

Tao J, Jiang W, Pan H, Xu X, Tang R (2007) Preparation of large-sized hydroxyapatite single crystals using homogeneous releasing controls. J Cryst Growth 308(1):151–158. https://doi.org/10.1016/j.jcrysgro.2007.08.009

Teaca CA, Rosu D, Mustata F, Rusu T, Rosu L, Rosca I, Varganici CD (2019) Natural bio-based products for wood coating and protection against degradation: A review. BioResources 14(2):4873–4901

Toy DF, Walsh EF (1987) Phosphorus chemistry in everyday living. Am. Chem. Soc., Washington, DC, United States

Trypuc M, Druzynksi S (2009) Investigation of mutual solubility in the NH4VO3-NH4NO3-H2O system. Ind Eng Chem Res 48(10):5058–5063. https://doi.org/10.1021/ie801341j

Van Hees P, Hertzberg T, Steen-Hansen A (2002) Development of a screening method for the SBI and Room Corner Test based on the Cone Calorimeter. SP report. 11

Velencoso M, Battig A, Markwart J, Schartel B, Wurm F (2018) Molecular firefighting - how modern phosphorus chemistry can help solve the challenge of flame retardancy. Angew Chem Int Ed 57(33):10450–10467. https://doi.org/10.1002/anie.201711735

Wang J, Shaw LL (2007) Morphology-enhanced low-temperature sintering of nanocrystalline hydroxyapatite. Adv Mater 19(17):2364–2369. https://doi.org/10.1002/adma.200602333

Wang F, Li M, Lu Y, Ge S (2005) Synthesis of nanocrystalline hydroxyapatite powders in stimulated body fluid. J Mater Sci 40(8):2073–2076

Wang F, Li M, Lu Y, Qi Y, Liu Y (2006) Synthesis and microstructure of hydroxyapatite nanofibers synthesized at 37°C. Mater Chem Phys 95(1):145–149

White RH, Dietenberger MA (2010) Fire safety of wood construction. In: Ross RJ (ed) Wood handbook—Wood as an engineering material. Gen. Tech. Rep. FPL-GTR-190. USDA Forest Service, Forest Products Laboratory, Madison, WI. Ch. 18.

Xiao X, Xiao X, Liu S, Li Y, Li Y, Li M (2024) Green and efficient flame-retardant nanocomposites from hydroxyapatite nanosheets modified porous wood. Ind Crops Prod 219. https://doi.org/10.1016/j.indcrop.2024.119105

Xin Y, Ando Y, Nakagawa S, Nishikawa H, Shirai T (2020) New possibility of hydroxyapatites as noble-metal-free catalysts towards complete decomposition of volatile organic compounds. Catal Sci Technol 10(16):5453–5459. https://doi.org/10.1039/d0cy00787k

Yang H, Yan R, Chen H, Lee D, Zheng C (2007) Characteristics of hemicellulose, cellulose and lignin pyrolysis. Fuel 86(12–13):1781–1788. https://doi.org/10.1016/j.fuel.2006.12.013

Yang J, Zhang S, Qian Y, Chen H, Peng Y, Yu Y (2024) Investigation into the performance enhancement of calcium phosphate mineralization-compacted Chinese fir. Forests 15(3). https://doi.org/10.3390/f15030452

Yasukawa A, Matsuura T, Nakajima M, Kandori K, Ishikawa T (1999) Preparation of nonstoichiometric calcium hydroxyapatite using formamide. Mater Res Bull 34(4):589–601

Yi L, Zhuang Y, Wang Z, Ding Y, Gong J, Liu C (2024) Experimental and numerical investigation on the combustion behavior of densified wood: Differences among wood species and impact of char oxidation. Fire Saf J 149. https://doi.org/10.1016/j.firesaf.2024.104245

Yu F, Ba Z, Gao Z, Wang Y, Xie Y, Wang H, Qiu Z, Xiao Z (2024) Modification with lignin-based N-P flame retardant to improve the flame retardancy and smoke suppression of wood. Chem Eng J 493. https://doi.org/10.1016/j.cej.2024.152827

Zhang H, Darvell B (2010) Synthesis and characterization of hydroxyapatite whiskers by hydrothermal homogeneous precipitation using acetamide. Acta Biomater 6(8):3216–3222. https://doi.org/10.1016/j.actbio.2010.02.011

Zhang Y, Lu J (2007) A simple method to tailor spherical nanocrystal hydroxyapatite at low temperature. J Nanopart Res 9(4):589–594. https://doi.org/10.1007/s11051-006-9177-3

Zhang Y, Lu J (2008) The transformation of single-crystal calcium phosphate ribbon-like fibres to hydroxyapatite spheres assembled from nanorods. Nanotechnology 19(15). https://doi.org/10.1088/0957-4484/19/15/155608

Zhang Y, Zhou L, Li D, Xue N, Xu X, Li J (2003) Oriented nanostructured hydroxyapatite from the template. Chem Phys Lett 376(3–4):493–497. https://doi.org/10.1016/S0009-2614(03)01038-8

Zhou Y, Qiu W, Zhou P, Wang Z, Zhang X, Mao X, Bu R (2024) Influences of species and density on the horizontal flame spread behavior of densified wood. Buildings 14(3):620. https://doi.org/10.3390/buildings14030620

Zhu K, Yanagisawa K, Onda A, Kajiyoshi K, Qiu J (2009) Morphology variation of cadmium hydroxyapatite synthesized by high temperature mixing method under hydrothermal conditions. Mater Chem Phys 113(1):239–243. https://doi.org/10.1016/j.matchemphys.2008.07.049